Available online at www.sciencedirect.com
ScienceDirect
Advances in Space Research 46 (2010) 208–220
ADVANCES IN SPACE RESEARCH (a COSPAR publication)
www.elsevier.com/locate/asr

Fading statistics and sensing accuracy of ocean scattered GNSS and altimetry signals

Scott Gleason *, Christine Gommenginger, David Cromwell

National Oceanography Centre Southampton, Empress Dock, Southampton, Hants SO14 3ZH, UK

Received 25 November 2009; received in revised form 12 March 2010; accepted 15 March 2010

Abstract

This paper starts with a brief review of scattering statistics theory for diffusely scattered radar signals. Following, global navigation satellite systems reflected (GNSS-R) signals are used to demonstrate the results of non-coherent signal averaging on the mean and standard deviation of the signal power fluctuations. The retrieved signal fading statistics of GNSS-R signals detected in low Earth orbit have been analyzed as a function of consecutive uncorrelated measurements (or looks) and instrument antenna gain and compared to the theoretical description presented by Ulaby, Moore and Fung for a radar remote sensing configuration. The results of this analysis include empirically determined error distributions that provide a reference to asses the potential accuracy of GNSS-R model based retrieval methods, and to what extent increasing the instrument antenna gain will improve the retrieval accuracy. Additionally, in assessing the potential of using GNSS-R signals for ocean remote sensing, it is useful to compare the signal characteristics with those of existing radar altimeter instruments. With this in mind, a fitting accuracy and parameter retrieval analysis has been undertaken using observed fading noise from successful space based altimeters. The noise observed on real waveforms has been added to a simulated ideal waveform with the intent to study the accuracy of ocean observables using a Monte Carlo simulation. By adding observed noise to ideal model waveforms in this way, it is possible to quantitatively asses the fitting errors with respect to noise variance contained in the least-squares model fitting sensing technique. Finally, the key differences between the traditional approach and the GNSS-R approach are then analyzed with regard to identifying the critical adjustments required in using GNSS-R signals for ocean remote sensing.

Keywords: GNSS-R; Remote sensing; Oceanography; Altimetry; Fading Statistics

1. Introduction

One of the crucial open questions in using GNSS-R signals for remote sensing, particularly with regard to altimetry applications, is the effect that fading noise on the detected power profile will have on the parameter retrieval accuracy. As summarized in the next section, signal fading due to diffuse scattering from a rough surface is a well known phenomenon that is traditionally mitigated using incoherent signal averaging. In essence, fading noise is an additional distortion added to the retrieved signal which corrupts the true shape of the power profile with random noise (or noise independent from the traditional electronic instrument noise). In attempting to perform remote sensing using a theoretical model, as is the case in traditional altimetry, there will also be imperfections in the model which will introduce errors independent of the noise on the signal. In other words, the expected signal return and how it relates physically to the surface will never be perfect. Nevertheless, theoretical models have been proven to provide a valid approximation for predicting surface parameters from radar power return profiles.

In order to perform a detailed analysis on signal fading in the GNSS-R case, several signals sampled at a raw intermediate frequency (IF) have been post-processed extensively on the ground. In the first case, two signals were selected for the fact that reasonable in-situ information

* Corresponding author. Tel.: +44 1483 532968.
E-mail address: sg26g08@noc.soton.ac.uk (S. Gleason).

0273-1177/$36.00 © 2010 COSPAR. Published by Elsevier Ltd. All rights reserved.
doi:10.1016/j.asr.2010.03.023

was available and the signals provided good examples of the calm sea and rough sea general cases. The second group of three signals were selected as they all exhibited weak received power levels and presented samples to demonstrate the dependance of signal statistics on signal to noise ratio, and by inference antenna gain.

This processing generated detailed fading statistics as a function of both delay across the surface and incoherent averaging duration or number of averages looks (where each look normally consists of a coherent 1ms correlation). The statistics of these signals exhibited the expected fading behavior for an ocean scattered signal. For consecutive uncorrelated returns, the single-look power distribution was clearly of an exponential form, which gradually changed to a chi-square distribution as consecutive waveforms were incoherently averaged together. After incoherent averaging times comparable to those used in traditional altimetry returns, the fading noise reduced to acceptable levels for use in surface parameter retrieval. As in the traditional altimetry case, parameter retrieval using GNSS-R signals can be performed using a model fitting technique. A reasonable understanding of how accurate the fitting procedure is can be explored using traditional altimetry waveforms and models.

The challenge of understanding the statistical properties of surface scattering has been an important subject in remote sensing research since its beginnings. Several decades ago (Fischer, 1972) published a description of the statistical distribution of measurements as received from a space orbiting instrument. Following, a more detailed explanation of the phenomenon was presented in Ulaby et al. (1982) which is used as the basis of the analysis presented here. In the case of scattered GNSS signals, early work on the statistical properties of scattered GNSS signals, and their connection to retrieval accuracy, was put forward in Zuffada and Zavorotny (2001) and Hajj and Zuffada (2003). This work concentrated on the signals leading edge, which as they suggested and the analysis below shows, has different noise characteristics from the trailing edge. Additional significant work which included theoretical analysis of GNSS altimetry was published by Rius and Cardellach (2010) using measurements from aircraft.

An interesting GNSS altimetry application, not analysed in detail here, is the possibility under certain conditions of making altimetry measurements using the coherent carrier phase (Jin and Komjathy, 2010). This technique has been successful under conditions where the reflected signal contains a large coherent component, for example at a very sharp grazing angles (Beyerle et al., 2002; Cardellach et al., 2004). Importantly, as part of their analysis, the noise statistics as a function of grazing angle where observed giving valuable insights into the dynamic statistical nature of a reflected GNSS signal.

In the case of traditional altimetry, the parameter retrieval accuracy using theoretical modelling has been analyzed in Challenor and Srokosz (1989). However, within a theoretical evaluation it is often difficult to grasp how errors in the model fitting are affected by fading noise quantitatively. An alternative methods for looking at this problem is the use of a numerical simulation, or more specifically, a Monte Carlo simulation using empirically observed noise profiles and a truth model waveform. Tools for performing this analysis have been developed as part of the development of the altimetry re-tracking software for the Envisat altimeter (Cipolini et al., 2009). This is a common technique used in traditional altimetry to re-process the detected power waveforms on the ground to fine tune the parameter retrievals. Using a simulated altimeter waveform and added Gaussian noise, error estimates due to the model fitting technique for various parameter retrievals, including ocean surface height and significant wave height, can be generated.

In order to make a useful statement concerning the model fitting errors observed using altimetry waveforms to what could be expected in the case of GNSS bistatic remote sensing, the key differences between the signals needs to be understood. The primary difference is that an altimetry signal is a frequency compressed "chirp" on the order of nanoseconds resolution (Chelton et al., 1989) while a GNSS signal is continuous signal with a pseudo-random ranging code modulated on the carrier. The ranging code chip duration ranges from approximately 293 m in the case of GPS L1 C/A to as short as 29.3 m in the case of GPS L5, GPS L1 P(Y) and a number of Galileo signals. Achieving the equivalent accuracy as that of the much shorter altimetry pulse will require a significantly altered processing strategy for GNSS-R signals (Jin et al., 2005).

The validity of this analysis applies generally to signals that meet the following conditions. First, that the signal has been incoherently scattered from the surface, in other words the surface scattering is diffuse with minimal or no coherent phase present in the detected signal. Using the general rule of thumb presented in (Beckmann and Spizzichino, 1987) the surface height differences that constitute a rough surface in the GPS C/A code case works out to be 4.8 cm for a grazing angle of 30°, 2.7 cm for 60° and 2.4 cm for 90° (perpendicular to the surface) (Gleason, 2006). Second, this analysis was performed only on GPS C/A code signals. As discussed later, GNSS signals with higher chipping rates can expect additional improvements. However, this analysis can be applied to various antenna gains, including those greater or less than from the signals presented here, based on the theoretical formulas presented in Ulaby et al. (1982).

The experimental configuration of the signals presented here was as follows. The receiver antenna has a peak gain of 11.8 dBiC and is off pointing 10° behind the satellite, opposite to the normal satellite velocity vector. A detailed description of the receiver antenna pattern can be found in Gleason (2006). The signals were sampled at approximately 5.58 samples per C/A code chip, or at roughly 0.18 chips per sample. This analysis shows that a significantly higher sampling rate would be required to perform accurate altimetry measurements with GPS L1 C/A code. For all signals

presented here the coherent processing interval was 1ms with the incoherent averaging interval varying and stated explicitly for each of the signals presented below.

2. Signal fading

Fading is of critical importance in remote sensing applications that involve diffuse scattering from rough surfaces. Fading occurs as a result of constructive and destructive interference between transmitted radiation reflecting off different facets within the glistening or scattering zone. If we think of a single measurement or look at the surface (before any incoherent averaging takes place) and the ocean surface being frozen during the coherent collection interval, the effects of fading become easier to understand. Assuming the ocean is reasonably rough with respect to the incoming signal wavelength, the different heights and orientations of the waves over the glistening zone will shift the phases of the incident radar wave randomly. Some of these paths will destructively interfere and others will constructively interfere with the result being a randomly fluctuating power level received at the antenna of the satellite based instrument. If you were to take just one sample or look, the chances of obtaining an accurate measurement of the true signal power would be quite low due to this natural signal fluctuation. Fading is mitigated in remote sensing applications by incoherent averaging of consecutive uncorrelated looks until the underlying signal power profile can be accurately determined. A good review of diffuse signal scattering statistics in included in Ulaby et al. (1982), upon which the following analysis is based.

For the looks to be considered uncorrelated, the reflecting surface or the viewing geometry needs to change sufficiently so that the conglomeration of received phases at the instrument is distinctly different from the look before it. At low Earth orbit (LEO) altitudes the high velocity of the receiver (on the order of several km/s) results in a rapidly changing viewing geometry and a relatively quick decorrelation time between looks at the surface. The peak coherent correlation time of the signals detected from space have been estimated for GNSS-R signals to be on the order of 1 ms (Lowe et al., 2002; Gleason, 2006). If the receiver is moving faster the coherent correlation time will shorten and if it slows it will lengthen. But even in the case of a stationary receiver the sea surface movement will change sufficiently to decorrelate samples eventually. Starting from standard rough surface scattering theory, the expected single look probability distribution of a power-detected signal is expected to take the form of an exponential (Ulaby et al., 1982, Eq. (7.74)),

$$p(P) = \frac{1}{\overline{P}} e^{\frac{-P}{\overline{P}}} \tag{1}$$

for values of

$$P > 0$$

where, $p(P)$, the single look power probability distribution function (PDF); P, the processed signal power; $\overline{P}$, the mean value of the processed signal power.

The signal power returned at each look is calculated as the total power returned after a single coherent detection at a given delay, minus the average noise power. The individual 1ms signal powers are then normalized by the mean signal power calculated over all looks at the same delay. The normalized processed signal power at each look can be expressed as,

$$\langle P_n^\tau \rangle = \frac{P_n^\tau}{\overline{P}^\tau} \tag{2}$$

where, $\langle P_n^\tau \rangle$, the normalized signal power returned at delay τ and look n; τ, the signal delay; n, the look number (1, 2, 3, etc.); P_n^τ, the signal power at delay τ for a single look measurement n; $\overline{P}^\tau$, the mean signal power over all looks at a given delay τ.

Attempting to state it simply; $\langle P_n^\tau \rangle$ is the signal power after a single coherent look at a given delay, normalized by the mean processed signal power over all looks. The values of $\langle P_n^\tau \rangle$ for 1000 consecutive looks are then distributed to yield the probability distribution of the processed signal power, $p(P)$.

Using consecutive 1 ms looks, the distribution of the normalized power returned in the presence of noise can be shown to fit an exponential curve. As an example, the exponential probability distribution of a scattered GNSS-R signal is shown below at the maximum signal power delay in Fig. 1. Importantly, this phenomenon is valid only for a diffusely scattered signal, as discussed in the introduction. This behaviour will not be observed under very calm conditions or at low elevation angles where a significant coherent signal is present.

What is of primary importance is our ability to measure the signal power accurately from one look or measurement

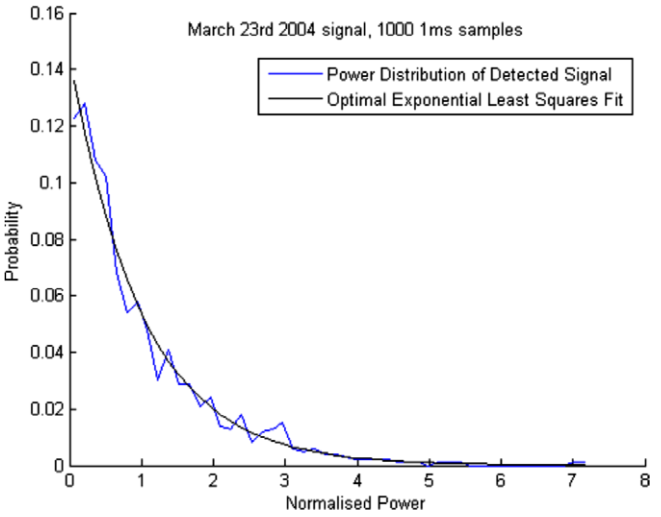

Fig. 1. Exponential power distribution of 1000 of 1 ms looks for the March 23rd 2004 signal. Shown with best least squares fit exponential function.

to the next. In the normalized case above, we require that all the measurements fall as close as possible to 1 with the variance of the measurements around 1 being a good indication of the measurement integrity. For any given look in the above distribution the chances are quite low that it will fall near the mean signal power (which is 1 due to the normalization). However, the standard deviation of the individual measurements around the mean is expected to decrease as a function of the number of incoherently averaged looks. Given that the standard deviation is equal to the mean for an exponential distribution, the resulting formula follows (Ulaby et al., 1982, Eqs. (7.75b) and (7.85)),

$$\sigma = \frac{\overline{P}}{\sqrt{M}} = \frac{\sigma_1}{\sqrt{M}} \tag{3}$$

where, M, the number of averaged looks or summations; σ_1, the standard deviation using the distribution of single looks.

Eq. (3) was derived in the ideal case, in the absence of noise. However, when the presence of noise is considered in the analysis, the standard deviation as a function of looks includes an additional term based on the signal to noise ratio. The expression for the standard deviation of the total received signal (signal plus noise) is (Ulaby et al., 1982, Eq. (7.100)),

$$\sigma_r = \frac{\overline{P}}{\sqrt{M}}\left(1 + \frac{1}{\Gamma}\right) \tag{4}$$

We are interested in the standard deviation of the signal power only, which follows directly from Eq. (4). The resulting expression for the standard deviation of the signal power as a function of the number of looks and the signal to noise ration is (Ulaby et al., 1982, Eq. (7.107b)),

$$\frac{\sigma_s}{\overline{P}} = \sqrt{\frac{\left(1+\frac{1}{\Gamma}\right)^2 + \left(\frac{1}{\Gamma}\right)^2}{M}} \tag{5}$$

The signal to noise ratio (SNR), Γ is defined as the amount the averaged processed signal power exceeds the averaged processed noise power, $\Gamma = \frac{\overline{P}}{\overline{P}_{noise}}$, where the noise power is calculated in the delay region before the start of the signal and the signal power is the total averaged power minus the averaged noise power. As Eq. (5) shows, after a certain point, increasing Γ will not significantly reduce the standard deviation of the measurements, acting in effect as a limit on the achievable improvement of the measurement standard deviation. For values of Γ below unity the measurement accuracy can be increased with increased power levels (with higher gain antennas, for example), but for values above unity the advantage decreases rapidly.

Finally, to achieve accurate surface sensing, it is desirable that consecutive measurements after incoherent averaging are consistent, or that nearly the same ocean surface is returning comparable values of signal power. The statistics between averaged measurements is our final indicator of the accuracy being achieved. The processed signal power after averaging M consecutive looks can be expressed as,

$$\langle P_Q^\tau \rangle = \frac{P_Q^\tau}{\overline{P}_Q^\tau} \tag{6}$$

where, $\langle P_Q^\tau \rangle$, the normalized signal power for measurement Q and delay τ; τ, the signal delay; Q, the measurement number, each of M consecutively summed looks; P_Q^τ, the signal power for measurement at delay τ; $\overline{P}_Q^\tau$, the mean signal power over all measurements Q at a given delay τ.

There are M independently summed looks in each measurement Q. The incoherent averaging process is expected to change the power distribution from exponential to chi-square as more and more summations are accumulated with the standard deviation decreasing according to Eq. (3). This is demonstrated in the following sections using reflected GNSS signals, where the signal power measurements used in the standard deviation calculations are calculated as per Eq. (6).

3. Fading statistics of GNSS-R signals

Two space detected GNSS-R signals have been processed in detail to examine their fading error characteristics. The first was collected on March 23rd 2004 over the ocean under calm conditions; the second signal was collected over the ocean under rough conditions on September 3rd 2004. For further details on the delay and Doppler power profiles of several ocean, land and ice reflected signals consult (Gleason et al., 2009; Gleason et al., 2005). The signals are shown in Fig. 2a and b over a range of delays across the surface. The delay waveforms for each of these signals are shown below for use as a reference, each of which was processed using 1ms coherent looks and 2 s of incoherent averaging.

As mentioned above, the coherent correlation time of 1ms used in processing a GNSS-R signal fortuitously agrees with the estimated scattered signal coherence time (Lowe et al., 2002; Gleason, 2006). However, we believe this is an area where more research is needed to better understand the affects of signal coherence on the processing and the final power waveforms. It is widely known that the signal coherence time will vary as a function of the scattering surface and sea roughness, and although using 1 ms will work as a first approximation, a better understanding of this phenomenon will help optimize the signal processing techniques in the future. For the signals described below, a 1 ms coherence correlation time was used to process individual looks throughout.

It is possible to quantify the noise on these signals by estimating the standard deviation of the fluctuations in the received waveforms. For the two signals presented above, the standard deviations of the noise at the peak

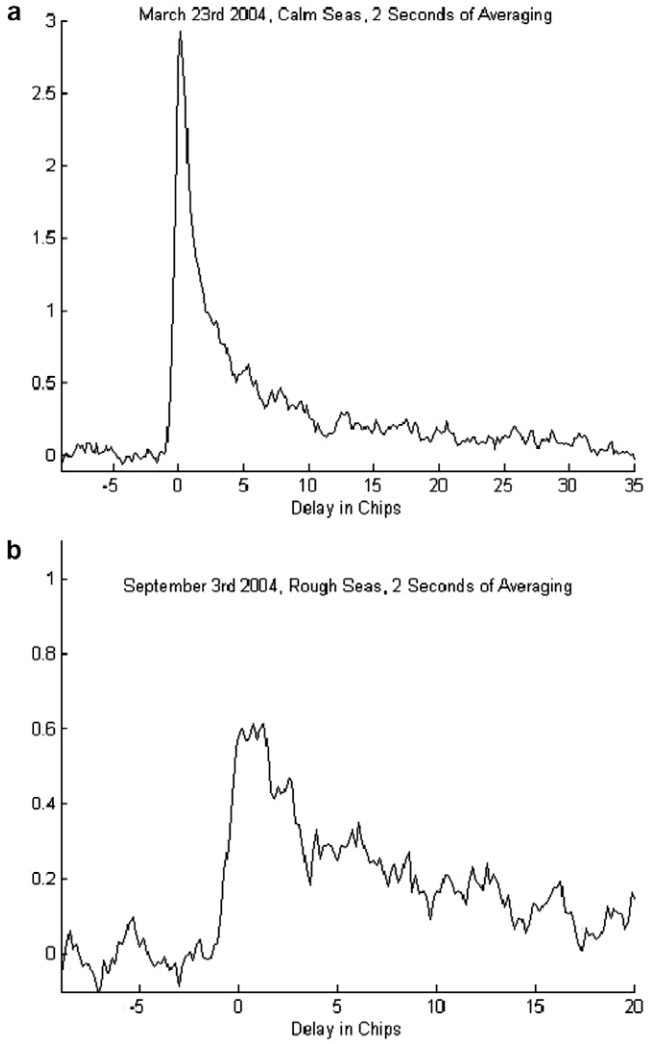

Fig. 2. Delay waveforms of the four example Earth reflected signals. (a) March 23rd 2004 over a calm ocean, (b) September 3rd 2004 over a rough ocean.

Table 1
The signal power distribution standard deviations at the maximum signal power delay bin after 1000 looks. The signal to noise ratio (SNR), wind speed and wave heights are added for reference.

Date	Wind speed (m/s)	Waves (m)	SNR Γ (dB)	Std
March 23rd 2004	≈3	N/A	1.36	1.60
September 3rd 2004	10.5	2.8 m	−5.39	3.74
no signal (Noise)	–	–	–	17.47

signal delays without any incoherent averaging are listed in Table 1.

The difference in received power from 1 millisecond to the next can differ significantly as expected, where even for a strong signal under calm conditions, significant power fluctuations occur. As more and more looks are averaged into the received waveform the signal power distribution changes from an exponential to chi-square (with correspondingly decreasing standard deviations).

The reduction in the standard deviation varies in both its rate of decrease with summations and the lowest standard deviation being converged upon between the different cases. The values shown in Table 2 were measured at the signal peak power delay. Note that there are approximately 5.58 samples per C/A code chip and the peak delay often falls between samples. The number of summed looks in the following tables are shown as a subscript to standard deviation σ.

Table 2
Standard deviation of processed signal power at the signal peak, t_{max}, computed for different numbers of independently averaged samples at the peak delay.

Date	σ_1	σ_5	σ_{10}	σ_{20}	σ_{50}	σ_{100}	σ_{200}
March 23rd 2004	1.6395	0.7858	0.5732	0.4339	0.2637	0.1697	0.1113
September 3rd 2004	4.3134	1.8329	1.2420	0.8432	0.5445	0.2927	0.1901

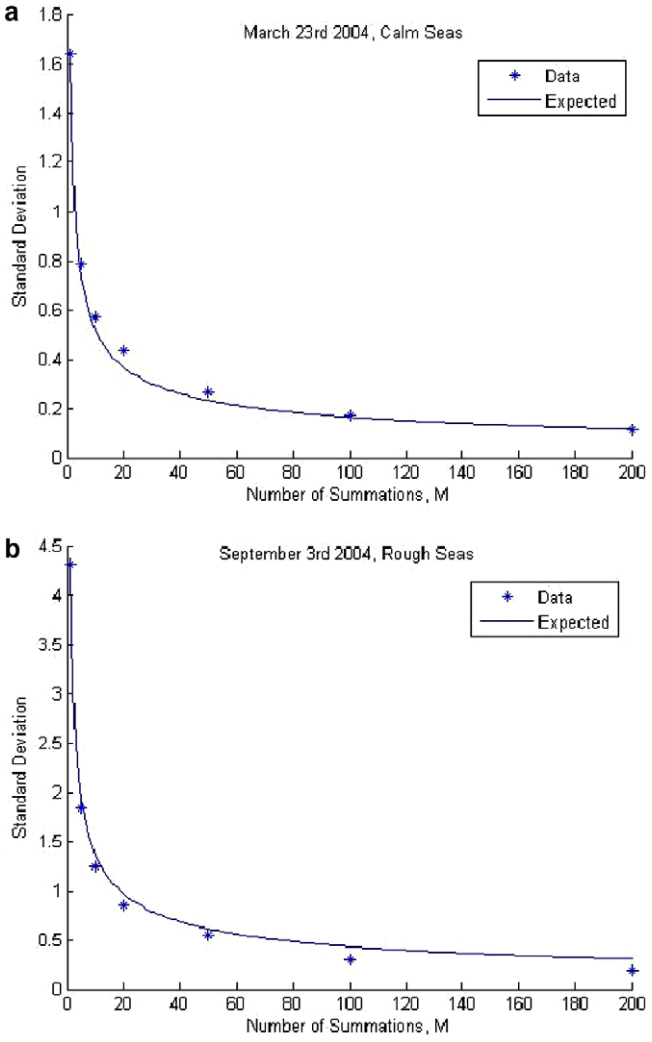

Fig. 3. Standard deviations vs. number of summations for each of the three example signals. (a) March 23rd 2004, (b) September 3rd 2004. The continuous curves show the expected decrease as per Eq. (3).

It is known that the standard deviation will decrease with the number of averaged samples as per Eq. (3). Fig. 3 illustrates the reduction in the signal power standard deviation vs. the number of samples M using the values in Table 2. The expected decrease in the standard deviation is plotted relative to the single look standard deviation, σ_1. The standard deviations decrease in a manner that is consistent with Eq. (3).

The two sample signals, as well as two additional reference signals (one over ocean swell and another over land) are shown together after 200 summations in the delay region around the specular reflection point in Fig. 4. All the signals have been aligned such that a C/A code delay of -1 is the best estimate of the delay at the start of the raising edge. Following, 0.0 would represent the specular point delay. It is understood that the specular reflection point will fall to the left (or earlier) than the peak signal power, which will occur somewhere to the right of center (Zavorotny and Voronovich, 2000; Zuffada and Zavorotny, 2001). However, the point of lowest standard deviations will provide the most favourable statistics for measurements. Notably in Fig. 4, the delay where the minimum standard deviations were observed corresponds roughly to the specular point delay (0.0 on the x-axis), which would be on the rising edge. The exception is the December 7th signal which was scattered from land, were the lowest standard deviation is even earlier on the rising edge. This would suggest that the optimal measurement statistics occur very close to the specular point delay on the rising edge.

The above examples were all collected under different ocean conditions and reflection geometries and as expected the summation process shows subtle variations in the overall results. The March 23rd signal under calm ocean conditions showed slightly lower overall standard deviations as a function of the summations than the rough sea signal of September 3rd. The signal collected under conditions of ocean swell was comparable to the rough sea case while the signal collected over land exhibited significantly larger errors at delays away from the specular reflection point.

The simplest way to improve the measurement accuracy in all these cases is to average for longer and longer intervals to further reduce the standard deviation as per Eqs. (3) and (5). The minimum standard deviations will be limited by the Cramer–Rao lower bound, determined by the minimum achievable variance of the signal noise over the longest allowable incoherent averaging interval (Kay, 1993).

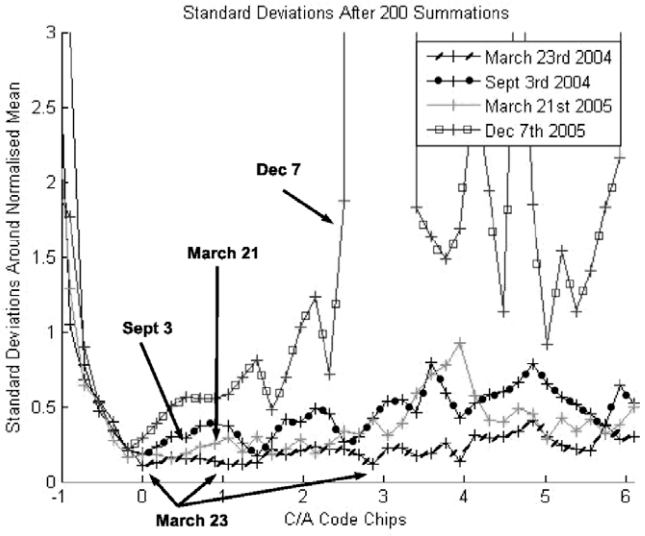

Fig. 4. Standard deviations as a function of delay after 200 of 1 ms summations for the three example signals. The C/A code spread between 1 and 1 represents the first iso-range ellipse on the surface. Calm ocean (March 23rd), rough ocean (September 3rd), ocean with swell (March 21st) and land (December 7th) (see Gleason (2006), for color image).

4. Signal statistics dependence on signal to noise ratio

Fischer (1972) has implied that the statistics of the signal will not benefit from a higher gain antenna. However, as described above, when Γ is less than unity, the signal power standard deviation σ_s is affected significantly by increasing Γ, which can be improved with a higher gain antenna. According to Eq. (5), this will only provide a improvement up to the point where Γ becomes significantly positive. This can be investigated using additional GNSS-R signals. Three signals have been identified that were collected under similar ocean conditions but received at different signal to noise ratios. The first two signals, those collected on July 22nd and 24th of 2005 were collected at almost identical incidence angles while another signal collected on November 21st 2005 was collected at a much lower incidence angle.

The wind and wave height information as estimated by the National Oceanic and Atmospheric Administration's National Data Bouy Center (NOAA, 2010) and measurements of the signal to noise ratio Γ are shown in Table 3. The values of Γ will determine the signal power standard deviation values for σ_s, as per Eq. (5). As the values of Γ for all three signals are significantly below unity we should expect a reasonable improvement as Γ increases.

My primary assertion here is that the statistics depend on Γ and that Γ is directly affected by the antenna gain. One can reasonably assume that for any given signal, if you raise the antenna gain by 1 dB, the Γ will raise by 1 dB, independent of everything else. This simplifies the

Table 3
GNSS-R data collections under similar ocean conditions but detected at different power levels. Additionally, the November 21st 2005 signal was collected at a significantly lower incident angle, which is believed to be related to the lower Γ observed.

Date	Wind (m/s)	Waves (m)	Angle (deg)	Γ (dB)	Gain (dB)
July 22nd 2005	8.0	2.1	32.5	−7.84	1.5
July 24th 2005	8.0	2.3	32.0	−2.38	9.8
November 21st 2005	10.0	2.2	2.5	−5.30	10.8

Table 4
Standard deviations of processed signal power at the delay, t_{max}, computed for different numbers of independently averaged samples. The value of M is shown as a subscript on σ.

Date	σ_1	σ_5	σ_{10}	σ_{20}	σ_{50}	σ_{100}	σ_{200}
July 22nd 2005	6.1544	2.7186	2.0178	1.3853	0.7758	0.6092	0.3550
July 24th 2005	2.9475	1.4150	1.0026	0.7362	0.5305	0.3932	0.2704
November 21st 2005	3.9546	1.8399	1.2195	0.8985	0.6393	0.4078	0.2444

analysis and allows us to use Γ alone to examine the signal statistics.

The results of repeating the fading analysis on the above three signals is shown in Table 4, where several values of the standard deviations and number of summations are listed. The decrease in standard deviation at the signal peak delay as a function of summations is clearly evident.

The decrease in standard deviation as a function of averaged samples is plotted below in Fig. 5 for all three cases at the peak power delay. From the plot below we can observe that at the estimated peak power delays the July 22nd signal (with lower antenna gain) has a higher standard deviation (i.e. larger measurement error) than the July 24th and November 21st signals (with higher antenna gains).

Plotting the signals together across a wider range of delays better illustrates the standard deviations dependence on delay for the three sample signals. Fig. 6 shows all three signals after 200 summations in the delay region around the signal peak.

The results on the signal rising edge approaching the peak are similar for all three signals. It is estimated that the peaks of the signals could be in error by a sample in either direction resulting in a greater separation between respective curves. On the trailing edge (delays >0), as the signal power is decreasing, there is a noticeable increase in measurement integrity with increasing antenna gains. At delays far from the peak, as the signal weakens, the increased signal to noise ratio Γ does help considerably.

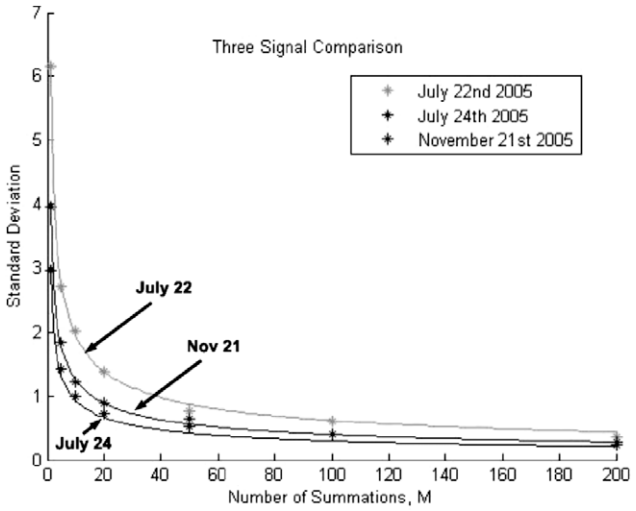

Fig. 5. Standard deviations as a function of consecutive summations for the July 22nd, July 24th and November 21st 2005 signals. The stars are the data points of Table 4 and the solid curves are the expected exponential decrease per Eq. (3). Absolute signal to noise ratios [upper −7.84] [middle 5.30] [lower 2.38] (see Gleason (2006), for color image).

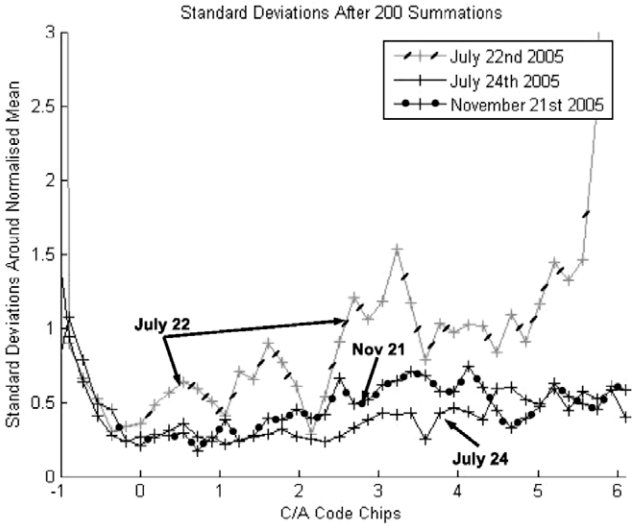

Fig. 6. Standard deviations as a function of delay after 200 summations for the three example signals. The C/A code spread between 1 and 1 represents approximately the first iso-range ellipse on the surface. The July 22nd 2005 signal was averaged over 3 s. The July 24th and November 21st 2005 signals were averaged over 2 s. Signal to noise ratios [upper -7.84] [middle 5.30] [lower 2.38] (see Gleason (2006), for color image).

Increasing the instrument antenna gain (in an effort to increase Γ) and fine tuning the processing to better match the optimal coherent correlation time will both aid to improve parameter retrieval accuracy with respect to the signals shown above. However, a low or medium gain antenna is probably sufficient for a scatterometer based empirical parameter retrieval (and even desirable due to their large surface footprint). For more demanding applications such as ocean altimetry, increasing the antenna gain with respect to that of the signals presented here (where the instrument antenna gain was 12dB) will increase the measurement accuracy, particularly under rough sea conditions. As predicted by Eq. (5), when the signal to noise ratios are significantly less than unity an increase in antenna gain will result in increased measurement accuracy. The rate of improvement will increase according to Eq. (5), with little or no advantage in increasing the value of Γ to significantly more than unity (Ulaby et al., 1982).

5. Comparison of GNSS-R with traditional altimetry

5.1. Traditional altimetry model summary

Spaceborne radar altimetry has been a valuable tool in environmental remote sensing for nearly 30 years. At present, radar altimeters such as Jason-1 and Envisat are pro-

viding continuous measurements over the Earth's oceans on a daily basis. The underlying concepts of their operation have been documented in detail by Chelton et al. (1989). The traditional altimetry method has been designed around the practical difficulties of transmitting and receiving very short duration (on the order of nanoseconds) pulses. To overcome this challenge, all recent altimeters have resorted to using long duration chirps with the same frequency content as the idealized pulse (Chelton et al., 1989). Consequently, the instrument predicts the anticipated return of the transmitted chirp and produces a second chirp at this time. The mixing of these two signals result in a combination which is a function of the frequency misalignment. Using discrete Fourier Transforms (DFT) on board the satellite to convert the signal into the time domain and then incoherently averaging several returns results in the final received waveforms, such as those shown in Figs. 7 and 8. For these examples, the pulse compression technique results in a received bin width of 3.125 ns. The features of this waveform contain information on the scattering surface, in particular the sea surface height is a point on the waveform raising edge and the significant wave height is a function of the slope of the leading edge. These parameters are normally estimated by fitting a theoretical model to the received waveform, as described next.

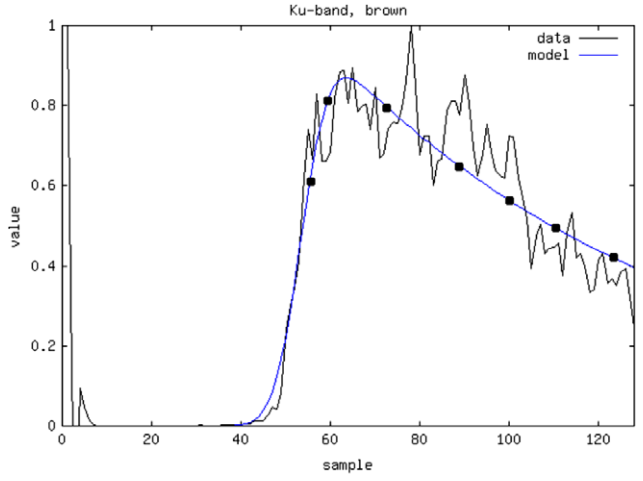

Fig. 7. Example of EnviSat Ku-band altimetry normalized waveform fitting under rough sea conditions. Signal shown has been averaged over 100 looks on-board the satellite (see Table 5).

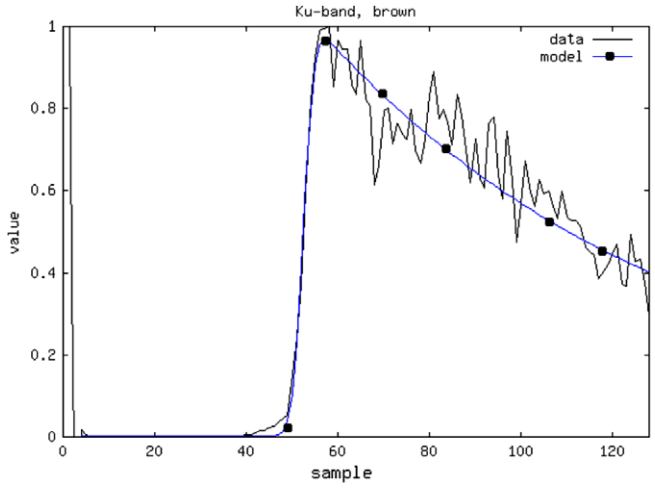

Fig. 8. Example of EnviSat Ku-band altimetry normalized waveform fitting under calm sea conditions. Signal shown has been averaged over 100 looks on-board the satellite (See Table 5).

5.2. Sensing ocean parameters

The received waveform is often compared with the return signal power time profile predicted by Brown (1977) to sense the surface. This predicted waveform is the convolution of three terms: The point target response P_{PT}, the flat surface response P_{FS} and the probability distribution function $q(\zeta)$ of the heights of the reflecting surface. The resulting power signal response, including the convolution of these three terms is shown below. For more details on the basic form see Quartly and Srokosz (2001) or including an expanded version of $q(\zeta)$ to include terms such as ocean wave skewness see Challenor and Srokosz (1989),

$$P(t) = P_{PT}(t) * P_{FS}(t) * q(\zeta) \tag{7}$$

Assuming that the emitted pulse can be approximated by a Gaussian function, and if the PDF of the reflecting facets is also Gaussian, the waveform will resemble those of Figs. 7 and 8. Referring to these figures, taken under different ocean conditions, the best-fit model waveforms where arrived at using a least squares fitting procedure. It should be noted that least-squares is only one of many possible fitting techniques, maximum likelihood or weighted least squares are others. Least squares was chosen for this analysis based on its wide use and simple implementation.

According to the theoretical basis of the Brown model, when the sea conditions are rough, this will be reflected in a more gradual slope of the raising edge as seen in Fig. 7, as contrasted to the sharper raise shown under the calm conditions illustrated in Fig. 8. This degree of roughness is reflected in the leading slope by the significant wave height (SWH) model input parameter. Importantly, the "center" of the raising edge gives an estimation of the sea surface height. This is effectively using the returned radar pulse to make a range measurement off the reflecting sea surface. The estimate of the surface height t_0 is often considered the primary observable of a radar altimeter.

The accuracy of the resulting parameter estimation can be estimated based on the received signal statistics (Challenor and Srokosz, 1989). However, as a reference truth for comparison with real measurements is not available, there is some uncertainty as to how well the model fitting procedure is estimating ocean characteristics. Inaccuracies in the surface parameter retrieval will fall primarily into two categories: (1) errors in the fitting procedure and (2) errors in the underlying model assumptions. This analysis will concentrate on model fitting errors only, while possible errors in the model itself have been examined in Challenor

and Srokosz (1989). The first step in assessing the accuracy of using a least squares fitting procedure is to obtain quantitative numbers for the statistical properties of the received waveforms, as was performed in detail for the GNSS-R case above.

5.3. Typical altimetry waveform noise statistics

Both of the received waveforms shown in Figs. 7 and 8 contain fading or speckle noise, even after incoherently averaging 100 looks. This noise will degrade the parameter estimation to some degree, and the noise itself will be a function of the number of non-coherent samples averaged together as per Eqs. (3)–(5). The fading noise statistics of several retired and operational ocean altimeters was analysed by Quartly and Srokosz (2001). Unlike the bistatic case described above, the data waveforms from altimeters do not provide a flexible option for the number of non-coherently averaged samples. Instead the number of looks in the average waveform is established before-hand by the instrument configuration. Table 5 gives a good summary of the multiple altimeters, including bin width and number of averaged waveforms for each instrument.

Incoherent averaging of waveforms must be performed using statistically independent looks. In the case of traditional altimetry this is a function of the pulse repetition frequency (PRF). For example, the PRF of the EnviSat Ku-band altimeter is 1800 Hz, or slightly longer than 1 pulse every half a millisecond. This assumes that in the duration of 0.55 ms the sea surface from which the radar pulse reflects must contain different reflecting facets that are statistically independent. The orbit design of EnviSat ensures that this is the case. In the case of the GNSS-R signals discussed above, consecutive looks were averaged together at 1 ms intervals (or a PRF of 1000 so to speak), and given the different orbit geometry (which determined the rate at which the instrument traverses the surface) this was assumed to be sufficient (Gleason, 2006).

Table 5
Operating characteristics of several altimeters, taken from Quartly and Srokosz (2001).

Altimeter	Launch date	Alt (km)	Freq (GHz)	PRF (Hz)	No. bins	bin (ns)	No. looks
Seasat	27 June 1978	800	13.5	1020	60	3.125	100
Geosat	12 March 1985	800	13.5	1020	60	3.125	100
ERS-1	17 July 1991	784	13.8	1020	64	3.03	50
ERS-2	21 April 1995	784	13.8	1020	64	3.03	50
TOPEX Ku	10 August 1992	1334	13.6	4500	128	3.125	2 × 228
TOPEX C	10 August 1992	1334	5.3	1200	128	3.125	4 × 60
Poseidon	10 August 1992	1334	13.65	1700	60	3.125	86
GFO	10 February 1998	800	13.5	1020	128	3.125	100
Jason-1 Ku	December 2001	1334	13.6	1800	104	3.125	90
Jason-1 C	December 2001	1334	5.3	300	104	3.125	15
Envisat Ku	January 2002	784	13.6	1800	128	3.125	100
Envisat C	January 2002	784	3.2	450	64	6.25	25

5.4. Retrieval accuracy demonstration using monte carlo simulation

A Monte Carlo simulation was performed to assess the potential fitting accuracy for a traditional altimetery waveform under both calm and rough sea conditions. Initially, a truth waveform was generated using a Brown model signal power profile, under both rough (SWH = 8 m) and relatively calm (SWH = 2 m) conditions. The waveform sampling and bin width was based on the EnviSat Ku-band waveform, containing 128 bins at 3.125 ns separation.

After the generation of the truth waveform, the following steps were run over 1000 iterations in a Monte Carlo simulation.

1. Gaussian noise, applied roughly as per Fig. 7 of Quartly and Srokosz (2001) for the Poseidon altimeter, was added on a sample by sample basis across the entire truth waveform. Special attention is made to the changing of the noise level between the bins before the start of the waveform raising edge and the remainder of the returned signal power in later bins.
2. The simulated waveform with added noise was then fit using a non-linear least squares fitting technique. A sparse variant of the Levenberg–Marquardt algorithm contained in the levmar C fitting routines (Lourakis, 2010) was used to fit the simulated waveform to an ideal Brown model.
3. Upon convergence of the least squares fitting, we compared the estimated values for the sea surface height with the simulated truth waveform.

Examples of the simulated truth signal, the simulated truth signal with added noise and the resulting best-fit waveform are shown in Fig. 9a and b for calm and rough seas respectfully.

The sea surface height parameter estimation results of the Monte Carlo simulation are shown in Fig. 10a and b for the calm and rough sea cases. As expected the error distribution for the fitting process is approximately Gaussian with zero mean. Additionally, the errors are greater in the rough sea case which is caused by the "stretching" of the raising edge. This stretching is even more exaggerated in the GNSS-R case where the rising edge of the signal spans approximately 30–300 m depending on the signal used.

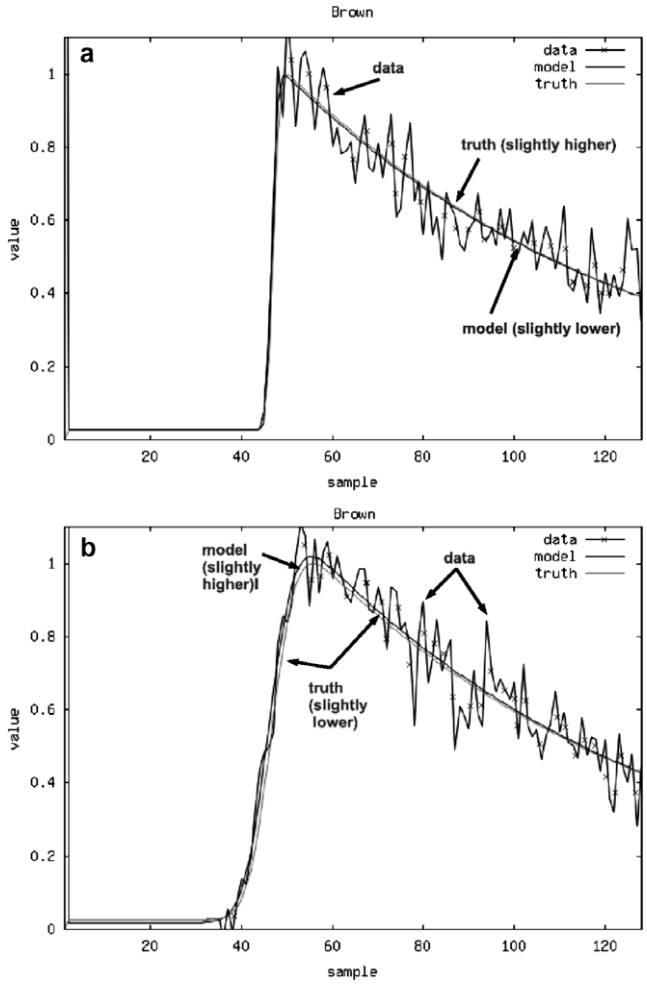

Fig. 9. Simulated waveforms with noise, resulting Brown model waveform fit and simulated waveform without noise (truth reference). (a) Truth waveform generated with significant wave height of 2 [truth is slightly above model], (b) truth waveform generated with significant wave height of 8 [truth is slightly below model].

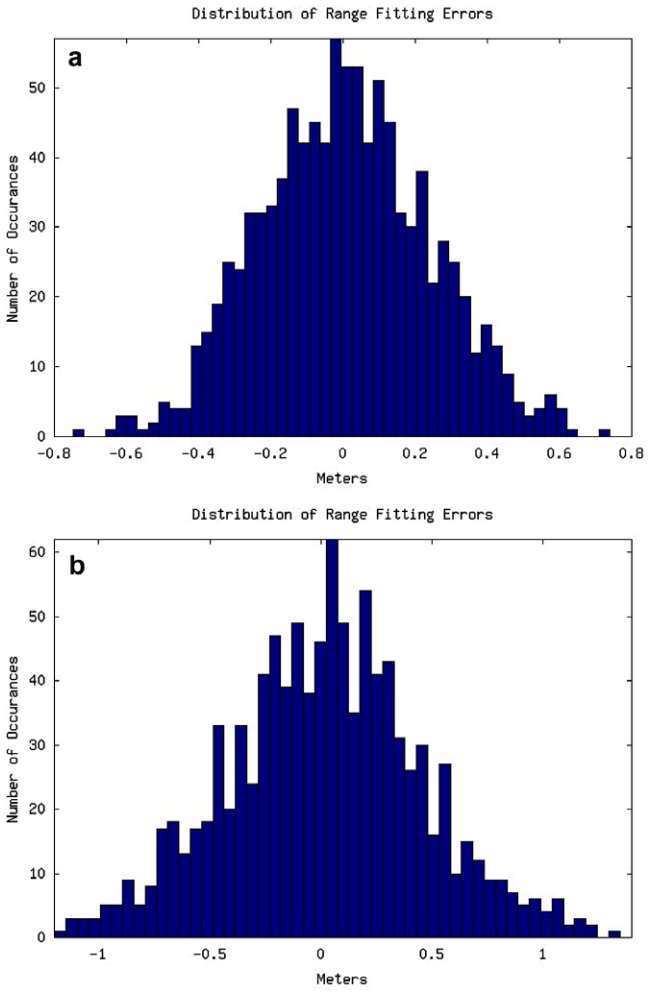

Fig. 10. Monte Carlo sea surface height error distribution for calm and rough sea cases. (a) Truth waveform generated with significant wave height of 2, (b) truth Waveform generated with significant wave height of 8.

5.5. Comparison between traditional altimetry and GNSS-R waveforms

In order to obtain insights into if the parameter retrieval error distribution achieved for altimetry could be replicated for a GNSS-R signal, the key differences between the two signals need to be studied. It must be kept in mind that GNSS signals are designed for use in terrestrial navigation applications where a direct line of sight is assumed between the satellite and the receiver. As such, certain design considerations beneficial to navigation, but not necessarily ocean remote sensing, are inherent in the signals themselves.

The Table 6 presents a quick comparison of the EnviSat Ku-band altimeter and an instrument designed for using GNSS-R signals, illustrating some of the key differences. Each of the differences listed in Table 6 is briefly discussed below.

5.5.1. Frequency

It is well established that there are difficulties in using L-band to sense ocean surface wind. This is primarily due to the L-band wavelength (19 cm in the case of the GPS L1 C/A signal) being too long to sense immediate changes in ocean waves, and hence surface wind speed consistently. Higher frequency wind instruments, such as QuickScat, have demonstrated this point (Freilich, 1999). However, an L-band signal will sense a large portion of the ocean surface waves, which in itself is a valuable observable. The potential of a GNSS-R instrument to sense ocean waves has been demonstrated from a space platform in Gleason (2006), where the difficulties in attempting to robustly sense wind using L-band were also encountered.

Conversely, L-band does not present any inherent obstacles to performing altimetry measurements. Additionally, L-band is known to have significant advantages in applications such as soil moisture sensing and sensing ocean salinity. The radiometer to be used on the European

Table 6
Comparison of EnviSat radar altimeter with a GNSS-R instrument.

Parameter	EnviSat	GNSS-R signal
Frequency (GHz)	Ku-band (13.575)	L1 (1.57542 GHz)
	S-band (3.2)	L2 (1.2276 GHz) L5 (1.17645 GHz)
Sampling bin width (ns)	Ku-band (3.125) S-band (6.25)	Variable
Effective width of rising edge	≈10 m	≈293 m (GPS L1 C/A code) ≈29.3 m (GPS L5, L1 P(Y)) See Fig. 11
PRF (pulse repetition frequency)	Ku-band (1800)	Approximately 1000
	S-band (450)	Using 1 ms looks
No. incoherently averaged waveforms	Ku-band (100)	Variable
	S-band (25)	(suggested 100–200)
Transmit and received power levels	Known	Very weak Not known exactly by users
Measurement biases	Corrected	Corrected

Space Agency's Soil Moisture and Ocean Salinity (SMOS) mission includes an L-band instrument (ESA, 2010).

5.5.2. Sampling bin width and width of rising edge

An important consideration in analyzing the noise on an ocean reflected waveform is to consider the statistical independence of the noise between sampling bins. In other words, from sample to sample in the data waveforms of Figs. 7 and 8, the fading noise must be uncorrelated. Or again, the ocean facets that return the power to bin X must be different than the facets that return power to bin $X+1$.

If the sampling rate is kept the same with respect to an altimetry signal this will result in minimally a 29.3 times worse accuracy for GPS C/A code signals, or 2.93 times worse for GPS L5 or L1 P(Y) signals for example. However, for the case of a GNSS-R signal with an approximately 293 m "pulse", an extreme over-sampling of the raising edge will be required in order to obtain sufficient bin resolution. These samples must be statistically independent for the least squares fitting technique to arrive at an unbiased estimate. It can be observed by examining the bistatic waveform model that the power in consecutive samples is highly correlated due to the spreading symbol (Zavorotny and Voronovich, 2000). Additional details on this and other inherent characteristics of GPS signals can be found in Misra and Enge (2001). However, as this is accounted for in the model generation, the underlying noise from sample to sample on the received signal power will be determined by the facets on the scattering surface and should be statistically independent, as is the case for an altimetry pulse. Therefore, in attempting altimetry with a GNSS-R signal the practicalities of sampling the raising edge at approximately the same resolution as an altimeter must be achieved.

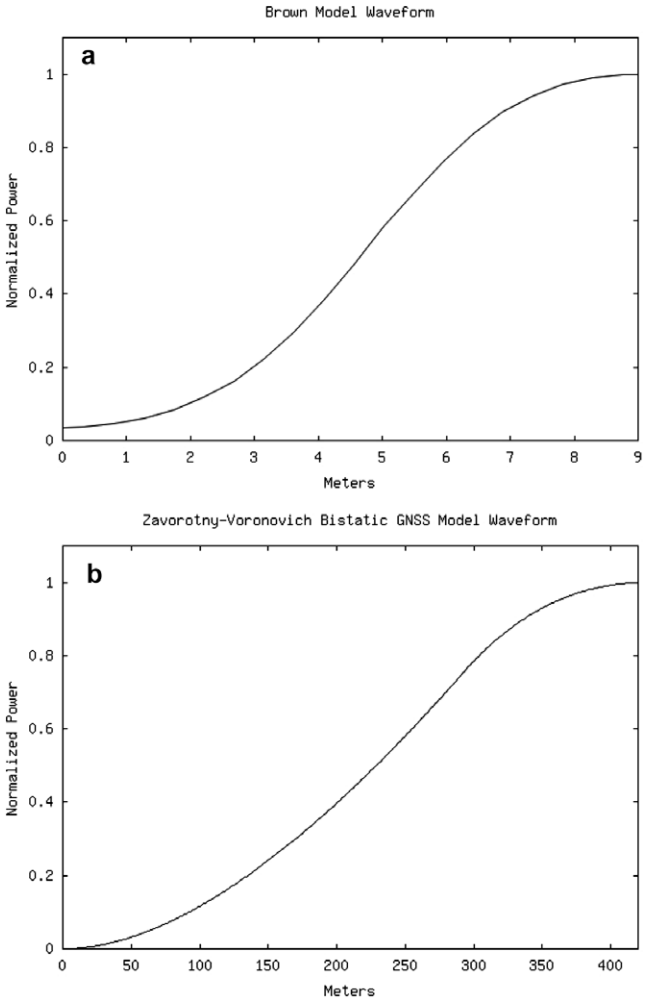

Fig. 11. Leading edge of an example (a) Brown model altimetry waveform and (b) a Zavorotny–Voronovich model GNSS-R waveform.

The second significant challenge in making an altimetry measurement with a GNSS-R signal is overcoming the additional stretching of the rising edge. Fig. 11 below shows a side by side comparison of a typical altimeter waveform with a GNSS-R waveform over the duration of the leading edge. As could be observed from the two altimetry Monte Carlo simulations, the retrieved accuracy is degraded by the stretching of the rising edge due to the increasing sea roughness. In the GNSS-R case the signal is significantly longer by design. The GNSS-R case can be viewed roughly as trying to perform waveform fitting on an extremely exaggerated altimetry waveform. This drop in accuracy is due to the fitting being more sensitive in the horizontal axis as the slope of the waveform increases. This issue presents a serious challenge and will require innovated fitting techniques to preserve the accuracy of the retrievals with a leading edge that can extends up to 400 m.

5.5.3. Pulse repetition frequency

The pulse repetition frequency (PRF) is the rate at which a traditional altimetry instrument transmits chirps. The PRF is designed so that consecutive chips return looks that are uncorrelated with each other. These looks are then averaged into the final power waveform profile used during the model fitting process. In the case of a GNSS-R signal, the signal power is spread across a frequency bandwidth and needs to be despread to recover the signal power, which is intentionally below the noise floor. In the case of the GPS L1 C/A code the correlation interval is 1ms, which is the normal coherent integration time needed to despread the signal power. Correlating for less than 1ms would result in a large loss of received power and make remote sensing with the signal problematic. Fortuitously, it has been estimated in Lowe et al. (2002) and Gleason (2006) that 1ms is on the order of the scattered signal coherence time. Therefore, assuming a 1 ms coherent correlation interval, a PRF of effectively 1000 would be reasonable for a GNSS-R instrument. Importantly, by altering the instrument orbit the scattered signal coherence time can be increased or decreased by design. As mentioned, shorter coherent correlation intervals result in a rapid power drop off, but longer correlation intervals could in theory increase the power SNR through higher correlation gains. As an example, assuming the satellite orbit has been designed so the signal remains coherent for 2 ms, a 2 ms coherent correlation would result in an effective PRF of 500.

5.5.4. Number of averaged waveforms

Figs. 3 and 5, as well as Table 5, illustrate that there is some flexibility on the number of looks that can be incorporated into the average waveforms used in model fitting. Referring to Table 5, for traditional altimeters these include values as low of 25 for the EnviSat S-band waveforms, with a more typical value of 100 for the EnviSat Ku-band altimeter. For the GNSS-R case, the optimal number will be as the noise standard deviation curves begin to plateau, after which averaging will provide only minimal improvements. Figs. 3 and 5 show that typically after 100 looks are incoherently averaged the noise standard deviations are starting to flatten out as per Eq. (3). Incoherent averaging beyond 100 in the GNSS-R case would yield better results in some conditions but would come at the cost of decreased measurement resolution.

5.5.5. Power levels

The transmit power levels of the GNSS signals, as broadcast from the satellites, as well as the exact transmit antenna pattern are not accurately known by the instrument. Additionally, the signal power level at the receiver is well below the ambient noise floor. These factors present problems for any parameter estimation based on an absolute power estimate, such as the traditional σ_0. Using σ_0 for empirically determining ocean waves, as attempted in Gleason (2006), requires detailed monitoring of the instrument automatic gain control (AGC) levels and good knowledge of the transmitting and receiving antenna patterns. To make matters worse, the basic transmit power level of a GPS signal fluctuates and is not openly published. Consider that a typical GPS receiver has very little interest in the absolute signal level, it may desire "more" power but the level itself is not used. Therefore, alternative methods need to be put in place to estimate the transmit signal power, such as monitoring the direct GNSS signal on the same instrument (note that the travel paths and viewing angles are different, so this will provide only an approximation), or creating a GNSS satellite power and antenna data base which is frequently updated and publicly accessible. In model based applications as described above, where the ocean sensing is attempted using the predicted signal shape only, the signal can be normalized, effectively obscuring the original power levels.

5.5.6. Measurement bias

Lastly, the estimated ocean height will be relative, in that there will be unknown (but hopefully slowly varying) biases on the range measurements (particularly due to the ionosphere and troposphere which can be several meters in magnitude). These errors will need to be corrected in post-processing as in the case of a traditional altimeter, where abrupt or unmodelled changes in the atmospheric delay of a GNSS-R signal (where every path for every signal is different) could introduce unexpected errors in the tracked ocean surface point.

6. Summary

This paper has presented a detailed analysis of the fading noise present on GNSS-R signals and how it can be mitigated using incoherent averaging and increasing signal power (to an extent). The resulting noise on the raw power waveforms will introduce errors during the estimation of ocean parameters. The errors introduced by signal fading into the least-squares fitting techniques have been simulated using fading statistics from exist radar altimeters, resulting in error distributions that generally reveal the expected accuracies of a radar altimeter. Following, the key differences between a radar altimeter and a GNSS-R instrument were discussed. For the case of making an ocean surface height measurement the key difference which affects the least-squares fitting procedure was found to be the elongated leading edge which increases by over an order of magnitude with respect to an altimeter waveform. This will present serious challenges to observing the ocean surface height using traditional model fitting techniques for GNSS-R signals. These difficulties arise due to the (a) increased sampling that will be required to obtain a comparable bin resolution with respect to useful altimeter bin widths and (b) the stretching of the leading edge is introducing a pseudo-roughness effect that will degrade the fitting accuracy and need to be overcome with innovative techniques.

The full range of GNSS-R applications have not been examined here and many are not faced with these obstacles, although each application has its challenges. For example, using GNSS-R signals to sense sea roughness (and under stable conditions surface wind) remains possibly the most feasible and worthwhile application. Additionally, study of how ice and land surface can be sensed using the GNSS-R technique is still in its relative early stages (Gleason, 2006). The difficulties in performing GNSS-R altimetry should not come as a surprise, for it could be expected that a signal designed primarily for terrestrial navigation will not meet all the requirements of a radar altimeter (where the designs of radar altimeters have been fine tuned over several decades). Altimetry will always be possible with a GNSS-R signal, it will just be a question of obtaining accuracies that are useful to the oceanography and remote sensing communities. An a final thought, we can look to another GNSS remote sensing application. GNSS radio occultation measurements have been shown to be extremely useful in environmental and meteorological applications, which were well outside the original signal design intentions. GNSS radio occultation measurements are being regularly incorporated into environmental models (Ao, 2009). In the future it is likely that GNSS-R remote sensing will also achieve greater success, but exactly in what areas is still being worked out.

References

Ao, C.O. Atmospheric sensing using GNSS radio occultations, in: Gleason, S., Gebre-Egziabher, D. (Eds.), GNSS Applications and Methods. Springer, Norwood, MA, ISBN 978-1-59693-329-3, 2009.

Beckmann, P., Spizzichino, A. The Scattering of Electromagnetic Waves From Rough Surfaces. Artech House, Norwood, MA, 1987.

Beyerle, G., Hocke, K., Wickert, J., Schmidt, T., Marquardt, C., Reigber, C. GPS radio occultations with CHAMP: a radio holographic analysis of GPS signal propagation in the troposphere and surface reflections. J. Geophys. Res. 107 (D24), 4802, doi:10.1029/2001JD001402, 2002, 2002.

Brown, G.S. The average impulse response of a rough surface and its applications. IEEE Trans. Antenn. Propag. 25 (1), 67–74, doi:10.1109/TAP.1977.1141536, 1977.

Cardellach, E., Ao, C.O., de la Torre Jurez, M., Hajj, G.A. Carrier phase delay altimetry with GPS-reflection/occultation. Geophys. Res. Lett. 31, L10402, doi:10.1029/2004GL019775, 2004.

Challenor, P.G., Srokosz, M.A. The extraction of geophysical parameters from radar altimeter return from a nonlinear surface, in: Brooks, S.R. (Ed.), Mathematics in Remote Sensing. Clarendon Press, Oxford, pp. 257–268, 1989.

Chelton, D.B., Walsh, E.J., MacAurther, J.L. Pulse compression and sea level tracking in satellite altimetry. J. Atmos. Ocean. Technol. 6, 407–438, 1989.

Cipolini, P., Vignudelli, S., Gommenginger, C., Snaith, H., Gleason, S., Coelho, H., Fernandes, F., Gmez-Enri, J., Martin-Puig, C., Woodworth, P., Dinardo, S., Benveniste, J. Advances in coastal altimetry: the COASTALT project outlook. In: Proceedings of the International Geoscience and Remote Sensing Symposium (IGARSS), July 12–17, Cape Town, South Africa. 2009.

ESA. European Space Agency Soil Moisture Ocean Salinity Mission Web Page. 2010.

Fischer, R. Standard deviation of scatterometry measurements from space. IEEE Trans. Geosci. Electronics GE-10 (2), 106–112, 1972.

Freilich, M.H. SeaWinds Algorithm Theoretical Basis Document. NASA Goddard Space Flight Center Web Site. 1999. http://eos-pso.gsfc.nasa.gov/.

Gleason, S., Hodgart, S., Yiping, S., Gommenginger, C., Mackin, S., Adjrad, M., Unwin, M. Detection and processing of bistatically reflected GPS signals from low earth orbit for the purpose of ocean remote sensing. IEEE Trans. Geosci. Remote Sens. 43 (6), 1229–1241, 2005.

Gleason, S. Remote Sensing of Ocean, Ice and Land Surfaces Using Bistatically Scattered GNSS Signals From Low Earth Orbit, Ph.D. Thesis, University of Surrey, 2006.

Gleason, S., Lowe, S., Zavorotny, V. Remote sensing using bistatic GNSS reflections, in: Gleason, S., Gebre-Egziabher, D. (Eds.), GNSS Applications and Methods. Artech House, Norwood, MA, ISBN 978-1-59693-329-3, 2009.

Hajj, G.A., Zuffada, C. Theoretical description of a bistatic system for ocean altimetry using the GPS signal. Radio Sci. 38, 10–11, 2003.

Jin, S.G., Komjathy, A. GNSS reflectometry and remote sensing: new objectives and results. Adv. Space Res. 46 (2), 111–117, 2010.

Jin, S.G., Wang, J., Park, P.H. An improvement of GPS height estimates: stochastic modeling. Earth Planets Space 57 (4), 253–259, 2005.

Kay, Stephen M. Fundamentals of statistical signal processing. Estimation Theory, Vol. I. Prentice Hall PTR, Upper Saddle River, New Jersey, ISBN 0-13-345711-7, 1993.

Lourakis, M. 2010. The Open Source Levmar Non-linear Least-squares Fitting Routines. Institute of Computer Science, Foundation for Research and Technology – Hellas.

Lowe, S., LaBrecque, J.L., Zuffada, C., Romans, L.J., Young, L.E., Hajj, G.A. First spaceborne observation of an earth-reflected GPS signal. Radio Sci. 37 (1), doi:10.1029/2000RS002539, 2002.

Misra, P., Enge, P. Global positioning system: signals, measurements, and performance. Ganga Jamuna Press, ISBN 0-9709544-0-9, 2001.

NOAA, 2010. The National Oceanic and Atmospheric Administrations's National Data Buoy Center.

Quartly, G.D., Srokosz, M.A. Analyzing altimetry artifacts: statistical properties of ocean waveforms. J. Atmos. Ocean. Technol. 18, 2074–2091, 2001.

Rius, A., Cardellach, E. Altimetric Analysis of the Sea Surface GPS Reflected Signals. IEEE Trans. Geosci. Remote Sens., doi:10.1109/TGRS.2009.2036721, 2010.

Ulaby, F.T., Moore, R.K., Fung, A.K. Microwave Remote Sensing: Active and Passive; Volume II: Radar Remote Sensing and Surface Scattering and Emission Theory. Artech House, Norwood, MA, 1982. ISBN 0-89006-191-2.

Zavorotny, V., Voronovich, A. Scattering of GPS signals from the ocean with wind remote sensing application. IEEE Trans. Geosci. Remote Sens. 38 (2000 951-96), doi:10.1109/36.841977, 2000.

Zuffada, C., and Zavorotny, V. Coherence time and statistical properties of the GPS signal scattered off the ocean surface and their impact on the accuracy of remote sensing of sea surface topography and winds. In: Proceedings of the IEEE International Geoscience and Remote Sensing Symposium. Sydney, Australia, 2001.